Contents lists available at ScienceDirect

Journal of Alloys and Compounds

journal homepage: www.elsevier.com

Doping induced dimensionality reduction of the magnetic order in $DyFe_{1-x}In_xO_3$

Ya Yang [a], Yabei Wu [a], Baojuan Kang [a], Zhenjie Feng [a], Jincang Zhang [a, b, c], Wei Ren [a, b, c, **], Shixun Cao [a, b, c, *]

[a] Department of Physics, and International Center of Quantum and Molecular Structures, Shanghai University, Shanghai 200444, China
[b] Materials Genome Institute, Shanghai University, Shanghai 200444, China
[c] Shanghai Key Laboratory of High Temperature Superconductors, Shanghai University, Shanghai 200444, China

ARTICLE INFO

Article history:
Received 25 August 2016
Received in revised form 28 October 2016
Accepted 31 October 2016
Available online xxx

Keywords:
Perovskite
Orthoferrites
Low-dimensional magnetism
Spin-reorientation

ABSTRACT

A series of $DyFe_{1-x}In_xO_3$ (x = 0, 0.1, 0.2, 0.3, 0.4, 0.5, 0.6, 0.7, 0.8, 0.9, 1) polycrystalline samples have been prepared by the conventional solid reaction methods. The crystal structures, refined by the Fullprof, are found to be orthorhombic for $0 \le x \le 0.6$ and hexagonal in the case of $0.7 \le x \le 1$. The lattice constants are changed by the In ions doping, and a huge distortion of the magnetic sublattice was induced. The magnetization versus temperature curves are obtained for all the samples, at the temperature between 3 K and 300 K. The pure $DyFeO_3$ sample undergoes a spin reorientation transition at around 50 K, whereas the doped In^{3+} ions significantly modify the phase transition. We reveal that such substitution retained the spin reorientation transition effect for $x \le 0.8$. We develop a formalism based on the molecular theory, giving explanation of the changes in the spin-reorientation temperature induced by the In-doping. Then, by performing density functional theory (DFT) calculation, we analyzed the magnetic phases for the hexagonal compounds. Furthermore, our findings indicate a type of Γ'_4 - Γ'_2 transition exists in the hexagonal Fe-In magnetic systems which directly point to a quasi-2 dimensional magnetic order.

1. Introduction

Perovskite rare-earth orthoferrites $RFeO_3$ (R is rare earth) have been investigated for their rich magnetic properties, dielectric properties, phase transitions and possible magnetoelectric multiferroic properties [1–7]. The $RFeO_3$ compounds have $GdFeO_3$-type distorted structure, mostly process spin reorientation transitions resulting from variation of the temperature and/or the magnetic field. These transitions induced by several complex interactions, expressed as Fe-Fe, R-R and R-Fe, have been attracting increasing attention recently. Among all $RFeO_3$, $DyFeO_3$ has been reported to have a coexistence of ferroelectricity and antiferromagnetism, which is important for functional spintronics materials [8–11]. Its transition is very unique, where the Fe^{3+} spins rotate from Γ_4 ($G_xA_yF_z$, the major antiferromagnetic vectors are along a axis with weak A-type antiferromagnetic order along b axis, and weak ferromagnetic component along c axis) to Γ_1 ($A_xG_yC_z$, antiferromagnetic component along b axis) at around 50 K. Generally, this transition is a kind of 3 dimensional ergodic phase transition, only dominated by the temperature and the magnetic field. With many excellent magnetic, electronic and optical properties, the $RFeO_3$ compounds can be applied to make laser-induced ultrafast spin reorientation (SR) [12,13], gigantic magnetoelectric coupling [14] and so on.

Recently, the low dimensional order has become a hot spot in magnetic materials research. Petit et al. confirmed the spin reorientation in the well-known hexagonal $RMnO_3$ originating from the striking spin-lattice coupling, where the in-plane Mn ions formed a two-dimensional (2D) magnetic order with in-plane spin reorientation transition [15]. Nath et al. presented a spin-1/2 compound CuP_2O_6 that featured a network of 2D antiferromagnetic square planes, interconnected via one-dimensional (1D) antiferromagnetic chains and the overall three-dimensional (3D) magnetic order is suppressed [16]. Additionally, in ferric oxides Kim et al. have determined a 2D spiral magnetic order of $Sr_3Fe_2O_7$ which offered an attractive platform for exploration of Skyrmion physics [17]. However, up to now, there are few reports on the hexagonal Fe magnetic orders in comparison to the mostly studied 3D spin reorientation in the rare-earth orthoferrites. Xu et al. performed first-principle calculations to predict structural, electric, magnetic and magnetoelectric properties of hexaferrites under chemical and hydrostatic pressures and pointed out a magnetic transition rendering the systems weakly ferromagnetic (0.03 μ_B for hexa-$DyFeO_3$) [18]. But we still know little about the influence of the 2D hexagonal lattice on the spin reorientation transition in such compounds.

In this paper, we introduced the nonmagnetic element indium (In) into $DyFeO_3$ system to substitute the iron (Fe) at the B-site. The hexagonal crystal $DyInO_3$ has the $P6_3cm$ space group, in which the Dy layers are divided by the InO_5 bipyramids forming a 2D layered structure [19,20]. Therefore, with the increasing In content, the $DyFe_{1-x}In_xO_3$ (x = 0, 0.1, 0.2, 0.3, 0.4, 0.5, 0.6, 0.7, 0.8, 0.9, 1) could undergo a crossing from 3D to 2D system which possibly has an impact on the spin reorientation transition. We also performed a first-principle calculations to study the electronic structure of layered $DyFe_{1-x}In_xO_3$ in order to reveal the effects of the In ions doping.

The paper is organized as follows. Section 2 provides details about the synthesis of the samples. The methods employed in our cal-

* Corresponding author. Department of Physics, and International Center of Quantum and Molecular Structures, Shanghai University, Shanghai 200444, China.
** Corresponding author. Department of Physics, and International Center of Quantum and Molecular Structures, Shanghai University, Shanghai 200444, China.
Email addresses: renwei@shu.edu.cn (W. Ren); sxcao@shu.edu.cn (S. Cao)

http://dx.doi.org/10.1016/j.jallcom.2016.10.321
0925-8388/

culations will be introduced in Section. 3. In Section. 4, we present our results of magnetism measurement and develop a phenomenological model to explain it. In Section. 5, the results of calculation are presented and discussed. Finally, we provide a summary in Section. 6.

2. Experimental

Polycrystalline samples $DyFe_{1-x}In_xO_3$ (x = 0, 0.1, 0.2, 0.3, 0.4, 0.5, 0.6, 0.7, 0.8, 0.9 and 1) were prepared by the conventional solid state reaction method, using the high-purity oxide powders Dy_2O_3 (99.9%), Fe_2O_3 (99.99%), and In_2O_3 (99.99%) (Sinopharm Chemical Reagent Co. Ltd.) as the starting materials. The stoichiometric mixture was pressed into pellets and sintered at 800 °C for 12 h. Then, the products were grinded and pressed into pellets of 13 mm in diameter and 2 mm in thickness at 12 MPa, and calcined at 1500 °C for 48 h. The crystal structures of the samples were examined by X-ray diffraction (XRD: D/max 2200 diffractometer, Cu-Kα radiation) at room temperature. The lattice parameters were obtained by the Rietveld refinement [21] calculation via Fullprof software [22]. The magnetic measurements were conducted on the Physical Property Measurement System (PPMS-9, Quantum Design Inc.). The measurements were performed to acquire the temperature dependence of the magnetization at the zero-field-cooling (ZFC) and field-cooling (FC) modes with a measurement field of 100 Oe.

3. Computational methods

In the present work, structure optimization and density of state (DOS) were carried out within DFT using the projected augmented wave (PAW) method as implemented in the Vienna ab initio Simulation Package (VASP) [23–25]. The Perdew-Wang (PW91) generalized gradient approximation was used as the exchange and correlation function [26]. Plane waves are included up to the kinetic-energy cutoff 550 eV. Additionally, structural optimization including lattice parameters and atomic coordinates are carried out until the Hellmann-Feynman force on each atom is less than 0.01 eV/Å and the stopping criterion for electronic self-consistent interactions is convergence of the total energy to within 10^{-5} eV. The 8 × 8 × 10 Monkhorst-Pack sampling method was used in the Brillouin-zone integration [27]. In order to obtain better accuracy, the semi-core states of Fe, In and Dy atoms are treated in the valence, 9 valence electrons for Dy ($5p^6 5d^1 6s^2$), 3 for In ($5s^2 5p^1$), 8 for Fe ($3d^7 4s^1$) and 6 for O ($2s^2 2p^2$) are treated in the calculation of electronic structure. We have kept the 4f electrons of Dy^{3+} ions frozen in the core shell, because partially filled f-states are not described well by density functional theory. And the ordered temperature of the rare-earth ion is mostly, in the rare-earth orthoferrites, under 10 K. For the rare earth orthoferrites, the correlation effect of localized d electrons should be necessarily considered. In this work, we use the DFT + U approach put forward by Dudarev [28], in which there is only one valid parameter for the effective Hubbard energy (U_{eff} = U-J). The U value of 3.2 eV [10] was set for both Fe and In atoms in our work. Furthermore, spin-orbit coupling (SOC) and non-collinear magnetism are considered to determine the energy of different magnetic configurations but not included in structural optimization.

4. Results and discussion

4.1. Structure of the samples

The phase and crystallinity of the as-prepared $DyFe_{1-x}In_xO_3$ (x = 0, 0.1, 0.2, 0.3, 0.4, 0.5, 0.6, 0.7, 0.8, 0.9, 1) samples were examined with XRD, as shown in Fig. 1. All the samples are phase-pure without any observable impurities. The diffraction patterns could be indexed with an orthorhombic perovskite structure (space group *Pnma*) for $x \leq 0.6$ and a hexagonal structure (space group $P6_3cm$) for $x > 0.6$, respectively. Regarding the crystal structure of $DyInO_3$, this compound is isostructural to the hexagonal $RMnO_3$ (R = Ho-Lu, Y). In Fig. 2 each In^{3+} ion is located inside an oxygen bipyramid with trigonal base, forming a pseudo-layered 2D structure by corner-sharing of the trigonal basal plane O atoms. The InO_5 bipyramids contain four kinds of nonequivalent In-O bonds. The R^{3+} ions are located between the InO_5 layers. Moreover, as shown in Fig. 2, the lattice parameters of $DyInO_3$ are a = 6.2439(1) (Å), c =

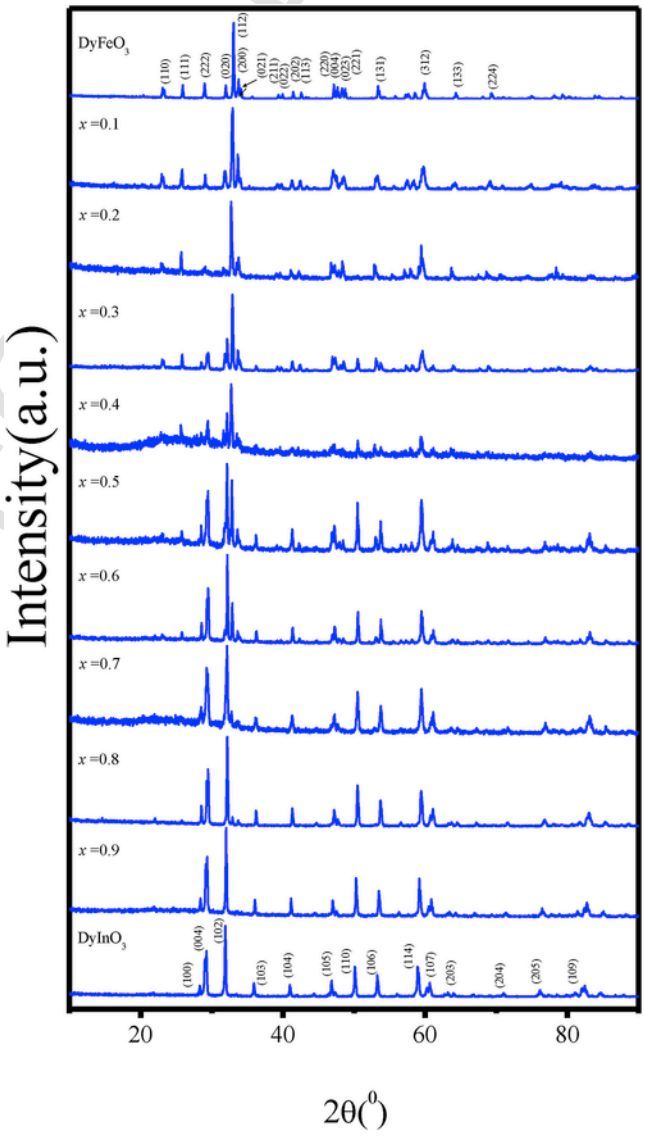

Fig. 1. X-ray diffraction patterns of $DyFe_{1-x}In_xO_3$ (x = 0–1.0 with an interval of 0.1).

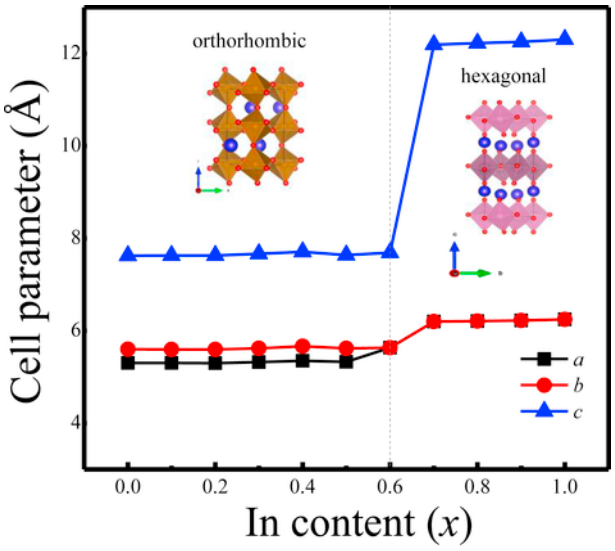

Fig. 2. Lattice parameters of $DyFe_{1-x}In_xO_3$ (x = 0–1.0 with an interval of 0.1) calculated from the XRD data.

12.1878(2) (Å), which are in good agreement with the literature [18,19]. While for the orthorhombic $DyFeO_3$, the parameters are a = 5.5957(1) (Å), b = 5.3009(1) (Å) and c = 7.6290(2) (Å). It is also shown in Fig. 1 that, when x changes from 0 to 1, the peaks featuring the orthorhombic $DyFeO_3$ around 30° gradually fade away, meanwhile the peak (102) of hexagonal $DyInO_3$ becomes apparent indicating a trend of structural phase transition by In-doping. In detail, our refined results presented in Fig. 2 show that the a, b and c parameters are not changed significantly in orthorhombic framework until x is up to 0.6. The structure transforms to the hexagonal framework in the case of $x > 0.6$, which offers a good example of the structural dimensionality reduction.

4.2. Magnetic analysis

For the pure $DyFeO_3$, a continuous phase transition of spin reorientation [5] occurs by varying temperature, as illustrated in Fig. 3. Without loss of generality, we have measured all the samples of x = 0–1 as seen in Fig. 3 (a)-(b). In detail, in the temperature range of 65 K–40 K, the $DyFeO_3$ magnetic configuration changes from the Γ_4 to the Γ_1 respectively, where the antiferromagnetic vector of Fe^{3+} sublattices rotates from the $\pm a$ axes (with a small canted moment to the c axis) to the $\pm b$ axes (with zero net magnetization). As displayed in Fig. 3(c), the M_H (M_L) indicates the maximum (minimum) value of the magnetization in the spin reorientation region. These values have largest magnitudes when x = 0.1, then decreases monotonically for $x > 0.1$. It is noted that when x = 0.7 and 0.8 the magnetic order might be changed to be in a 2D magnetic framework of the hexagonal crystal structure.

Overall, the total magnetic moment depends on In-doping concentration, especially when nonmagnetic ions doping in the antiferromagnetic system from x = 0 to x = 0.1. In the rare-earth orthoferrite, the substituting nonmagnetic ions destroyed the original canted antiferromagnetic Fe-Fe coupling and invoked an enhancement of the net moment. But as the concentration of nonmagnetic ions keeps increasing, the total moments monotonically decrease as shown in Fig. 3(c). Analogously, our result is coincident

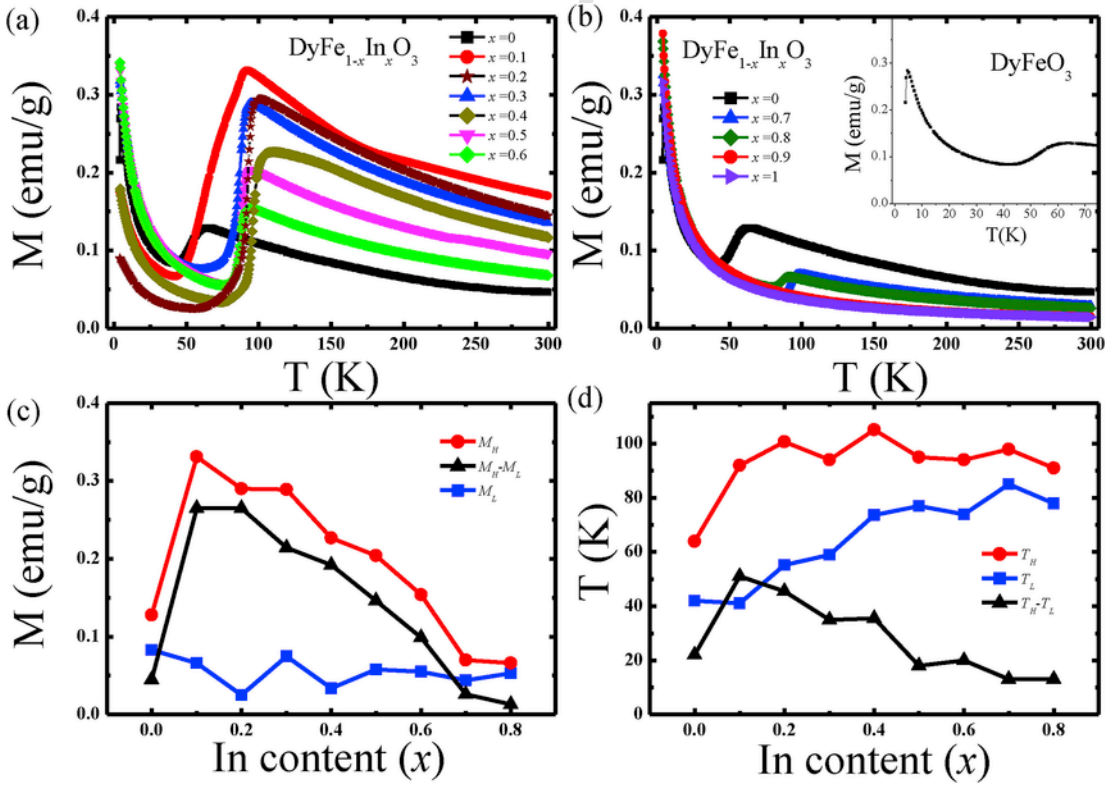

Fig. 3. ZFC magnetizations as function of temperature for $DyFe_{1-x}In_xO_3$ (a) x = 0, 0.1–0.6. (b) x = 0, 0.7–1.0. (c) The peak value of the higher magnetization in the spin reorientation range M_H and the valley value M_L as a function of x. (d) The higher and lower temperature of the spin reorientation range (T_H and T_L) as a function of x. The differences between M_H and M_L, and between T_H and T_L are also shown in (c) and (d).

with the previous report by Hong et al., who found the descending net magnetization in the $DyMn_{1-x}Fe_xO_3$ system and simultaneously broken canted antiferromagnetic structure for the excess Mn ions [29]. Especially in the $DyFe_{0.6}Mn_{0.4}O_3$, a spin reorientation transition was found to occur around 310 K which indicates an effective way to improve the transition temperature by modulating the magnetic order [30]. Interestingly, and different from their result of the disappearance of spin reorientation for the Mn content over 60%, we have observed here spin reorientation phase transition for x up to 80%. Furthermore, we reveal that even a small amount of In doping may destroy the magnetic order of Dy as observed in pure $DyFeO_3$ below 4.6 K. This can be seen clearly that the feature of downward turn in x = 0 M-T curve is absent for x = 0.1–1, see the inset of Fig. 3(b).

From Fig. 3(d), upon cooling, the T_L and T_H, denoted as the ending and beginning of the SR transition, both increase with the substituting amount by the In ions. The SR temperature of our pure $DyFeO_3$ is in accord with the single crystal results of Zhao et al. [31]. However, our polycrystalline sample shows a wider range of SR temperature between 40 and 65 K, in contrast to a sharp SR transition temperature at 50 K for single crystal. In order to explain the curves of T_L, T_H vs x, we adopt a formalism based on molecular field theory, to relate changes in the spin reorientation temperature to In-induced changes in the anisotropy field [32]. As the stable configuration for the Fe^{3+} spins depends on the relative magnitudes of the anisotropic portions of the magnetic free energy, we consider the magnetocrystalline anisotropy in the two terms,

$$-\sum_i \sum_\alpha A_{\alpha\alpha} m_{i\alpha}^2 - \sum_i \sum_{\alpha<\beta} A_{\alpha\alpha\beta\beta} m_{i\alpha}^2 m_{i\beta}^2 \tag{1}$$

where $A_{\alpha\alpha}$ describes the second-order anisotropy field and $A_{\alpha\alpha\beta\beta}$ is for the fourth-order anisotropy field. The α and β represent the a, b or c axis. It was confirmed that the antiferromagnetic vectors of Fe^{3+} sublattices lie along the ±α axes when

$$A_{\alpha\alpha} - A_{\beta\beta} > A_{\alpha\alpha\beta\beta}. \tag{2}$$

The doped In ions have an influence on the spin reorientation by producing changes in the anisotropy fields. Then, we may assume that $A_{\alpha\alpha}$ is analytic function of concentration x and temperature T. According to theory, for $DyFeO_3$ the in-plane portion of the second-order anisotropy,

$$K_{ab}(x,T) \equiv A_{aa}(x,T) - A_{bb}(x,T) \tag{3}$$

should pass through zero during a spin reorientation in the a-b plane. By carrying out a Taylor series expansion of $K_{ab}(x,T)$ in the neighborhood of a spin reorientation at concentration, x^0, and temperature, $T_{ab}(x^0)$, we find,

$$K_{ab}(x,T) = \left(x - x^0\right)\left(\partial K_{ab}/\partial x\right)_{x^0,T_{ab}^0} + \left(T - T_{ab}^0\right)\left(\partial K_{ab}/\partial x\right)_{x^0,T_{ab}^0} + \ldots \tag{4}$$

where the constant term, $K_{ab}(x,T)$, vanishes at the transition point.

$$K_{ab}\left(x, T_{ab}\right) = 0 \tag{5}$$

whence

$$\left(\frac{dT_{ab}}{dx}\right)_{x^0} = -\frac{\left(\partial K_{ab}/\partial x\right)_{x^0,T_{ab}^0}}{\left(\partial K_{ab}/\partial T\right)_{x^0,T_{ab}^0}} \tag{6}$$

This equation determines the slope of the curve $T_{ab}(x)$, i.e. $T_H(x)$ in our work, at $x = x^0$, in terms of the partial derivatives of K_{ab} with respect to x and T. Considering that In-In interaction for their closed shell of the $4d^{10}$ configuration is very small, we may assume the dependence of $A_{aa}(x,T)$ on concentration is linear. For $x < 0.1$, we express $A_{aa}(x,T)$ by the following formula,

$$A_{aa}(x,T) = (1-x)\,P_{aa}(T) + xQ_{aa}(T) \tag{7}$$

where $A_{aa}(0,T) = P_{aa}(T)$ is the case for the pure ($x = 0$) ferrite material, and the $xQ_{aa}(T)$ is due to the In-doping. Plugging these in the expression for dT_{ab}/dx, we get,

$$\left(\frac{dT_{ab}}{dx}\right)_{x^0} = \left(\frac{\left(Q_{aa} - Q_{bb}\right) - \left(P_{aa} - P_{bb}\right)}{\left(1-x^0\right)\left(P'_{aa} - P'_{bb}\right) + x^0\left(Q'_{aa} - Q'_{bb}\right)}\right)_{T_{ab}^0} \tag{8}$$

where the prime symbol in P' (Q′) denotes dP/dT (dQ/dT). Since $K_{ab}(x,T) = 0$, the P and Q coefficients in the numerator are constrained by the relation (7) above, which gives

$$\left(\frac{dT_{ab}}{dx}\right)_{x^0} = \left(1-x^0\right)^{-1}\left(\frac{Q_{aa} - Q_{bb}}{\left(1-x^0\right)\left(P'_{bb} - P'_{aa}\right) + x^0\left(Q'_{bb} - Q'_{aa}\right)}\right)_{T_{ab}^0} \tag{9}$$

At low doping concentrations in $DyFe_{1-x}In_xO_3$, i.e. the limit of $x^0 = 0$, it can be simplified as

$$\left(\frac{dT_{ab}}{dx}\right)_{x=0} = \left(\frac{Q_{aa} - Q_{bb}}{P'_{bb} - P'_{aa}}\right)_{T_{ab}^0} \tag{10}$$

The reorientation temperature increases linearly for very small x in proportion to the In anisotropy, Q_{aa}-Q_{bb}, and is inversely proportional to the derivative of the host anisotropy, P_{bb}-P_{aa}, with respect to temperature. In our case, the initial doped In ions introduce the In anisotropy and then the increasing nonmagnetic ions, the host anisotropy will drop down quickly which results in the increasing and then decreasing spin reorientation temperature. Therefore, the spin reorientation transition could remain the 3D ordering when $x \leq 0.6$. However, due to the change of lattice structure, the phase transition may show 2D features for $x > 0.6$.

Furthermore, stating from the $DyInO_3$ in which no spin reorientation occurs, we have a formalism to express the case as x approaches to $x = 1$ [32].

$$T_{ab} = (1/k)\log\left(x/x_c\right) \tag{11}$$

As previously mentioned, a spin reorientation in the α-β plane could happen, only if the $K_{ab}\left(x,T_{ab}\right)=0$ is satisfied. Based on that, a critical concentration x_c is defined and the k represents the strength of the perturbation to the anisotropy by the temperature. With equation (11), we can fit the T_L *vs* x curve in Fig. 4. From the fitting, the k is 0.04968 and the x_c is 0.01293. In Ref. [32], the authors found the x_c to be about 0.002 for the Co doped system, possibly because of the nonmagnetic In ions and the orthorhombic-hexagonal change of lattice structure.

5. DFT calculation

We employed the first-principle calculation to study the electronic structure of $DyFe_{1-x}In_xO_3$ compounds, by looking at the total density of states for the different doping concentration of In. Here we choose the DFO ($DyFeO_3$), $DyFe_{0.5}In_{0.5}O_3$, $DyFe_{1/3}In_{2/3}O_3$ (DFIO) and DIO ($DyInO_3$) as the representatives. Among those, the half-doping $DyFe_{0.5}In_{0.5}O_3$ was built according to the *Pnma* space group and the $DyFe_{1/3}In_{2/3}O_3$ was considered in the $P6_3cm$ group based on the XRD results.

The total density of states of the four structures are shown in Fig. 5. In the case of DFO, the half-filled 3d orbitals of Fe^{3+} ions constitute the occupied bands below the Fermi level and the empty bands above the Fermi level, indicating an insulating ground state. Different from the DFO, the In^{3+} ions in the DIO are full-filled with the 4d orbits, and the electrons are located below the Fermi level which produce a wider band gap. For the half doped $DyFe_{0.5}In_{0.5}O_3$, the full-filled In^{3+} ions have little influence on the electronic structure. It is easy to understand that the half-doped nonmagnetic In^{3+} ions simply double the orthorhombic cells of DFO in certain directions without changes of properties. While for the hexagonal DFIO, the distinct local environment around the Fe^{3+} ions will drastically change the density of states. As shown in Fig. 5, electronic states below and above the Fermi level produce an intermediate band gap.

In order to further analyze the magnetic configurations, we have done non-collinear magnetism calculation for the DFO and hexagonal DFIO which should present the spin reorientations in orthorhombic lattice and hexagonal lattice respectively. As mentioned, the magnetic order of DFO will undergo Γ_4 ($G_xA_yF_z$) to Γ_1 ($A_xG_yC_z$) transition. Since the Dy^{3+} ions get ordered under very low temperature of 5 K, we exclude the magnetism of 4f electrons in the calculation. As displayed in Fig. 6, the Γ_4 phase is reproduced to have the following magnetic moments in unit of μ_B: S_{Fe1} = (−4.071, −0.024, −0.021), S_{Fe2} = v(4.071, 0.024, −0.021), S_{Fe3} = (4.071, −0.024, −0.021), S_{Fe4} = (−4.071, 0.024, −0.021). The results suggest the existence of a net magnetization of 0.021μ_B per formula unit along the z axis, which is consistent with the result of 0.023 μ_B reported in Ref. [13] for $NdFeO_3$. Hence, the simulation of Γ_4 phase confirms the weak ferromagnetism originates from the Fe sublattice for $T > T_{SR}$. Upon cooling, the ferromagnetic moment gradually disappears as the Fe sublattice forms a Γ_1 ($A_xG_yC_z$) phase. Our first-principle calculations for Γ_1 phase produce the following magnetic moments in unit of μ_B: S_{Fe1} = (−0.021, 4.072, −0.015), S_{Fe2} = (0.021, −4.072, −0.015), S_{Fe3} = (−0.021, −4.072, 0.015), S_{Fe4} = (0.021, 4.072, 0.015). Indeed, there is no net magnetization for the Fe sublattice because all vectors are completely canceled along three axes.

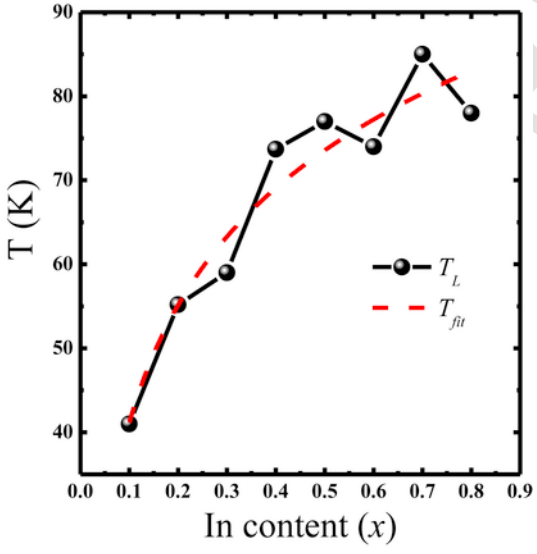

Fig. 4. The numerical fitting curve and data of lower temperature of spin reorientation range T_L *vs* x.

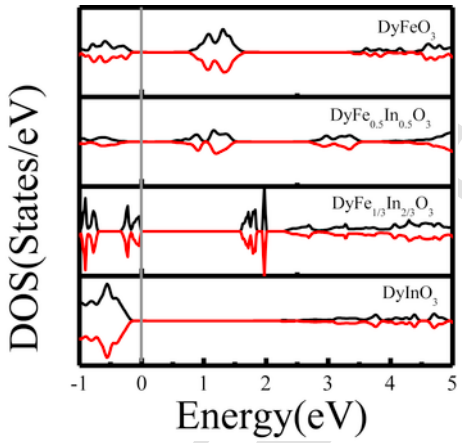

Fig. 5. Comparison of total DOS for DFO, $DyFe_{0.5}In_{0.5}O_3$, $DyFe_{1/3}In_{2/3}O_3$ and DIO. The vertical line indicates the Fermi level. All of the compounds show insulating ground states with finite band gaps.

In the hexagonal structure DIO, we substitute 2 out of 6 In^{3+} ions by 2 Fe^{3+} ions in a supercell. We found from computation that these 2 Fe must be located in two different hexagonal layers, in order to give a band gap as measured from experiments. According to Ref. [18], we examined several magnetic orders in hexagonal structure denoted as Γ'_1, Γ'_2, Γ'_3 and Γ'_4 phases. The lowest energy Γ'_2 produces the following magnetic moments in unit of μ_B: S_{Fe1} = (2.530, −0.023, −0.104), S_{Fe2} = (1.243, 2.203, −0.106). The moments in the *xy*-plane have larger components than that along the z axis, indicating the existence of an in-plane magnetic ordering. As shown in Fig. 7, we exhibited the four kinds of magnetic phases. For $T > T_{SR}$, the system may stay in a Γ'_4 phase with the highest energy as: S_{Fe1} = (0.031, 2.531, −0.064), S_{Fe2} = (2.208, −1.238, −0.063)μ_B. The energy difference between the Γ'_4 and Γ'_1 is about 0.8 meV, also in agreement with the Ref. [18]. Therefore, we suggest that when the temperature reaches the critical T_{SR}, the moments of the two iron ions would rotate 90° simultaneously, giving a Γ'_4–Γ'_2 transition. In addition, it was found that a long-range antiferromagnetic ordering could be developed by introducing 30% Fe content in Mn sites of $TbMnO_3$ and a spin reorientation transition also occurred [33]. The strong Fe-Fe coupling may induce a magnetic order even for a sparse Fe density. Our calculation results might be further inspected by the neutron diffraction experiments.

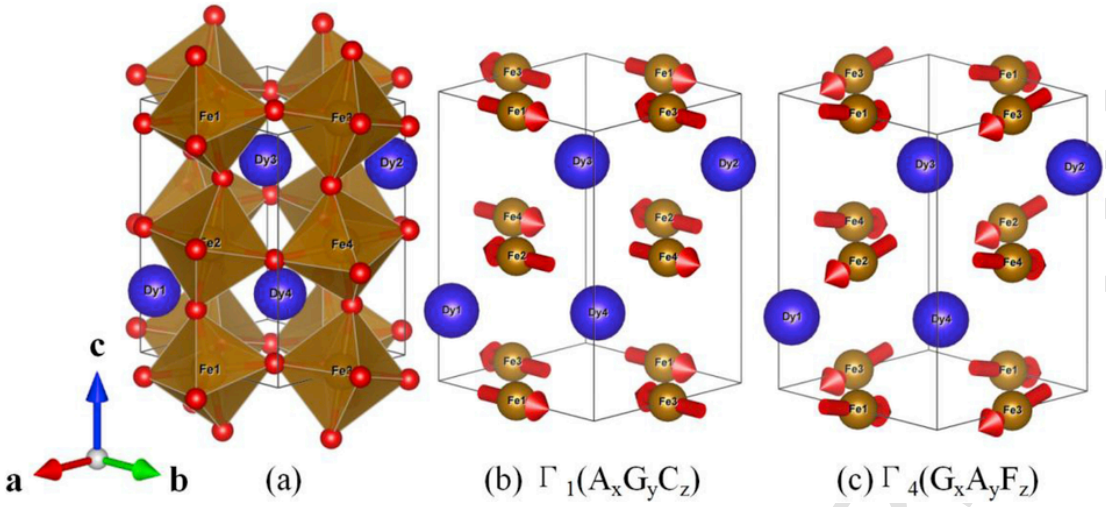

Fig. 6. (a) Crystal structure of the orthorhombic DFO. (b) Γ_1 phase and (c) Γ_4 phase magnetic configurations of DFO used in the calculations. The arrows express the schematic spin orientations for Γ_4 and Γ_1 phases.

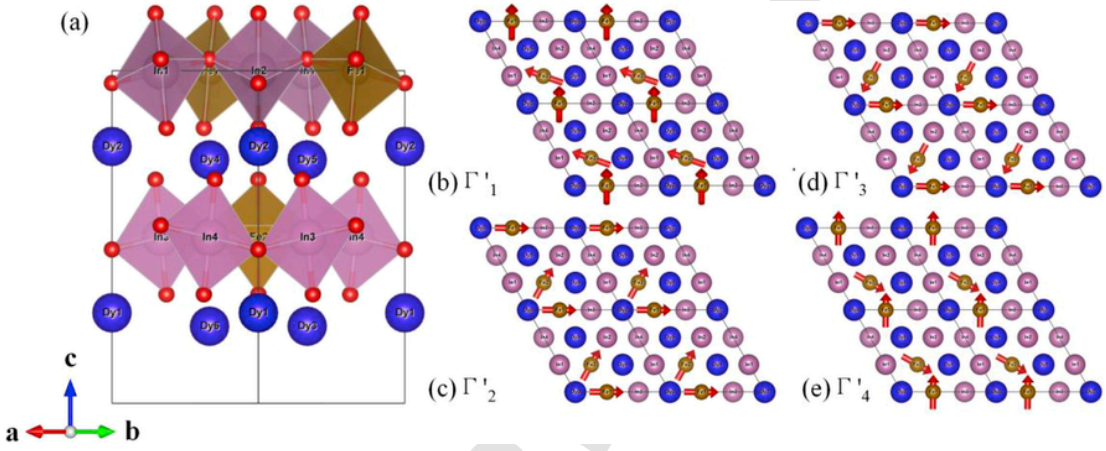

Fig. 7. (a) Crystal structure of the hexagonal DFIO. (b)–(e) show the allowed Γ'_1, Γ'_2, Γ'_3, and Γ'_4 phase magnetic configurations studied in the calculations. The arrows express the schematic spin orientations of the Fe ions for the four phases.

6. Conclusions

In summary, we have studied the magnetic properties and electronic structures of $DyFe_{1-x}In_xO_3$, especially the In^{3+} ions doping effects of the spin reorientation transition, using magnetic measurement experiments, molecular field theory, and the first-principle calculation. As the In-doping content increases, we found the structure of $DyFe_{1-x}In_xO_3$ would change from an orthorhombic perovskite to a hexagonal oxide at a critical concentration $x = 0.6$ which induced dimensionalities of the magnetic order decaying from 3D to quasi-2D. Consequently, the temperature of the spin reorientation transition, expressed as T_H and T_L in this work, increased due to the anisotropy field originating from the In^{3+} ions. Moreover, we employed a phenomenological formalism to explain the behavior, based on the molecular field theory. The magnitude of the spontaneous magnetization is enhanced first and subsequently reduced, by the increasing nonmagnetic ions doped into the canted antiferromagnetic system. In addition, we employed DFT calculations to study orthorhombic $DyFeO_3$ and $DyFe_{0.5}In_{0.5}O_3$ structures, along with the hexagonal $DyInO_3$. Moreover, the non-collinear calculations in the hexagonal $DyFe_{1/3}In_{2/3}O_3$ pointed out a quasi-2D order which show the in-plane spin reorientation transition with a special type of Γ'_4 to Γ'_2.

Acknowledgments

This work is supported by the National Natural Science Foundation of China (NSFC, Nos. 51372149, 11274221, 11274222, 11574194, 51672171), the National Key Basic Research Program of China (Grant No. 2015CB921600), QiMingXing and Pujiang Project (14QA1402000, 13PJD015) of Shanghai Municipal Science and Technology Commission, Eastern Scholar Program, Shuguang Program (Grant No. 12SG34) from Shanghai Municipal Education Commission. Special Program for Applied Research on Super Computation of the NSFC-Guangdong Joint Fund (the second phase), and Shanghai Supercomputer Center are also acknowledged.

References

[1] W.C. Koehler, E.O. Wollan, M.K. Wilkinson, Phys. Rev. 118 (1960) 58–70.
[2] Shixun Cao, Huazhi Zhao, Baojuan Kang, Jincang Zhang, Wei Ren, Sci. Rep. 4 (2014) 5960.

[3] Shujuan Yuan, Yabin Wang, Mingjie Shao, Fenfen Chang, Baojuan Kang, Yosikazu Isikawa, Shixun Cao, J. Appl. Phys. 109 (2011) 07E141.
[4] Hailong Wu, Shixun Cao, Ming Liu, Yiming Cao, Baojuan Kang, Jincang Zhang, Wei Ren, Phys. Rev. B 90 (2014) 144415.
[5] Weiyao Zhao, Shixun Cao, Ruoxiang Huang, Yiming Cao, Kai Xu, Baojuan Kang, Jincang Zhang, Wei Ren, Phys. Rev. B 91 (2015) 104425.
[6] Hui Shen, Zhenxiang Cheng, Fang Hong, Jiayue Xu, Shujuan Yuan, Shixun Cao, Xiaolin Wang, Appl. Phys. Lett. 103 (2013) 192404.
[7] Fang Hong, Zhenxiang Cheng, Shujun Zhang, Xiaolin Wang, J. Appl. Phys. 111 (2012) 034104.
[8] V.V. Eremenko, S.L. Gnatchenko, N.F. Kharchenko, P.P. Lebedev, K. Piotrowski, H. Szymczak, R. Szymczak, Europhys. Lett. 11 (1987) 1327–1331.
[9] L.A. Prelorendio, C.E. Johnson, M.F. Thomas, B.M. Wanklyn, J. Phys. C. Solid St. Phys. 13 (1980) 2567–2578.
[10] Alessandro Stroppa, Martjin Marsman, Georg Kresse, Silvia Picozzi, New J. Phys. 12 (2010) 093026.
[11] Ryugo Iida, Takuya Satoh, Tsutomu Shimura, Kazuo Kuroda, B.A. Ivanov, Yusuke Tokunaga, Yoshinori Tokura, Phys. Rev. B 84 (2011) 064402.
[12] A.V. Kimel, A. Kirilyuk, P.A. Usachev, R.V. Pisarev, A.M. Balbashov, T. Rasing, Nature 435 (2005) 655–657.
[13] S.J. Yuan, W. Ren, F. Hong, Y.B. Wang, J.C. Zhang, L. Bellaiche, S.X. Cao, G. Cao, Phys. Rev. B 87 (2013) 18.
[14] Y. Tokunaga, S. Iguchi, T. Arima, Y. Tokura, Phys. Rev. Lett. 101 (2008) 097205.
[15] X. Fabreges, S. Petit, I. Mirebeau, S. Pailhes, L. Pinsard, A. Forget, M.T. Fernandez-Diaz, F. Porcher, Phys. Rev. Lett. 103 (2009) 067204.
[16] R. Nath, K.M. Ranjith, J. Sichelschmidt, M. Baenitz, Y. Skourski, F. Alet, I. Rousochatzakis, A.A. Tsirlin, Phys. Rev. B 89 (2014) 014407.
[17] J.-H. Kim, Anil Jain, M. Reehuis, G. Khaliullin, D.C. Peets, C. Ulrich, J.T. Park, E. Faulhaber, A. Hoser, H.C. Walker, D.T. Adroja, A.C. Walters, D.S. Inosov, A. Maljuk, B. Keimer, Phys. Rev. Lett. 113 (2014) 147206.
[18] Changsong Xu, Yurong Yang, Shanying Wang, Wenhui Duan, Binglin Gu, L. Bellaiche, Phys. Rev. B 89 (2014) 205122.
[19] Tetsuya Tohei, Hiroki Moriwake, Hidenobu Murata, Akihide Kuwabara, Ryo Hashimoto, Tomoyuki Yamamoto, Isao Tanaka, Phys. Rev. B 79 (2009) 144125.
[20] Chuanlong Lin, Jing Liu, Yanchun Li, Xiaodong Li, Rui Li, Solid State Commun. 173 (2013) 51–55.
[21] H.M. Rietveld, J. Appl. Cryst. 2 (1969) 65.
[22] J. Rodriguez-Carvajal, Phys. B 192 (1993) 55.
[23] G. Kresse, J. Hafner, Phys. Rev. B 47 (1993) 558.
[24] G. Kresse, J. Hafner, J. Phys. Condens. Matter 6 (1994) 8245.
[25] G. Kresse, J. Furthmller, Phys. Rev. B 54 (1996) 11169.
[26] J.P. Perdew, J.A. Chevary, S.H. Vosko, K.A. Jackson, M.R. Pederson, D.J. Singh, C. Fiolhais, Phys. Rev. B 46 (1992) 6671.
[27] H.J. Monkhorst, J.D. Pack, Phys. Rev. B 13 (1976) 5188.
[28] S.L. Dudarev, G.A. Botton, S.Y. Savrasov, C.J. Humphreys, A.P. Sutton, Phys. Rev. B 57 (1998) 1505.
[29] Fang Hong, Zhenxiang Cheng, Hongyang Zhao, Hideo Kimura, Xiaolin Wang, Appl. Phys. Lett. 99 (2011) 092502.
[30] Hui Shen, Zhenxiang Cheng, Fang Hong, Jiayue Xu, Xiaolin Wang, Jianli Wang, Zhenyin Yu, Yuanxu Wang, J. Alloys Compd. 680 (2016) 226.
[31] Z.Y. Zhao, X. Zhao, H.D. Zhou, F.B. Zhang, Q.J. Li, C. Fan, X.F. Sun, X.G. Li, Phys. Rev. B 89 (2014) 224405.
[32] L. Holmes, L.G. Van Uitert, Richard Hecker, J. Appl. Phys. 42 (1971) 657–663.
[33] Fan Hong, Binbin Yue, Jianli Wang, Andrew Studer, Chunsheng Fang, Xiaolin Wang, Shixue Dou, Zhenxiang Cheng, Appl. Phys. Lett. 109 (2016) 102401.